Effect of H_3BO_3 on the phase stability and long persistence properties of $Sr_{3.96}Al_{14}O_{25}:Eu^{2+}_{0.01}$, $Dy^{3+}_{0.02}$ phosphor*

Xie Wei(谢 伟)[a)b)c)], Wang Yin-Hai(王银海)[c)†], Zou Chang-Wei(邹长伟)[a)], Liang Feng(梁 枫)[a)], Quan Jun(全 军)[a)], Zhang Jun(张 军)[a)], and Shao Le-Xi(邵乐喜)[a)]

[a)] *Development Center for New Materials Engineering & Technology in Universities of Guangdong, Zhanjiang Normal University, Zhanjiang* 524048, *China*
[b)] *School of Physics and Engineering, Sun Yat-Sen University, Guangzhou* 510275, *China*
[c)] *School of Physics and Optoelectronic Engineering, Guangdong University of Technology, Guangzhou* 510006, *China*

(Received 23 June 2012; revised manuscript received 7 December 2012)

$Sr_{3.96}Al_{14}O_{25}:Eu^{2+}$,$Dy^{3+}$ long persistent materials with different weights of H_3BO_3 prepared by the high temperature solid-state reaction method were characterized by X-ray powder diffraction (XRD), scanning electronic microscopy (SEM), photoluminescence spectra (PL), and thermoluminescence (TL). The results of XRD indicate that the 3% addition of H_3BO_3 favorable for the formation of pure phase $Sr_4Al_{14}O_{25}$, and $SrAl_{12}O_{19}$ was generated when there is a low content or high content of H_3BO_3. The average grain sizes of samples grow bigger with an increase of H_3BO_3. PL spectra show that the emission peak does not shift evidently and the emission intensity changes little, indicating that the different amount of H_3BO_3 has little influence on the crystal field. The decay characteristics and TL measurement show that H_3BO_3 affects the afterglow properties of $Sr_{3.96}Al_{14}O_{25}:Eu^{2+}$,$Dy^{3+}$, because the increasing H_3BO_3 leads to more defects in the $Sr_4Al_{14}O_{25}$ matrix.

Keywords: phosphor, afterglow, luminescence, thermoluminescence

PACS: 61.05.cp, 78.20.−e, 33.50.Dq, 66.30.Ma **DOI:** 10.1088/1674-1056/22/5/056101

1. Introduction

Rare-earth doped long persistence materials have been widely studied,[1–9] due to their many advantages, such as high luminescent brightness, long afterglow time, good chemical stability, and environmental friendliness. Alkaline earth aluminates are one of the best hosts for rare-earth ions. One typical rare-earth ion doping in alkaline earth aluminates is $SrAl_2O_4:Eu^{2+}$, Dy^{3+} which was successfully synthesized by Matsuzawa.[10] $SrAl_2O_4:Eu^{2+}$, Dy^{3+} emits a green light peaking at 520 nm due to the 5d-4f transition of Eu^{2+} ions.[11] The 5d–4f transition is associated with the change in electric dipole and the 5d excited state is affected by the crystal field effects, so the emission of Eu^{2+} is very strongly dependent on the host lattice and can occur from the ultraviolet to the red region of the electromagnetic spectrum.[12] Thus, the luminescence of Eu^{2+} is different when it is doped in different host structures. Another typical rare-earth ion doping in alkaline earth aluminates is $Sr_4Al_{14}O_{25}:Eu^{2+}$, Dy^{3+} which have high quantum efficiency and shows superior persistence properties than $SrAl_2O_4:Eu^{2+}$, Dy^{3+}. In general, H_3BO_3 was added into raw materials when synthesizing strontium aluminates.[13–16] For example, an appropriate amount of H_3BO_3 was added to raw materials when the authors synthesized $SrAl_2O_4:Eu^{2+}$, Dy^{3+},[17] and the effect of H_3BO_3 on the structure and photoluminescence properties of phosphors was discussed. However, the influence and the mechanism of H_3BO_3 in the phosphor are not clearly complete. In Refs. [13], [15], and [18], H_3BO_3 was also used when the authors synthesized $Sr_4Al_{14}O_{25}:Ce^{3+}$ or $Sr_4Al_{14}O_{25}:Eu^{2+}$, Dy^{3+}, but the amount of H_3BO_3 is not very accurate. The results of Refs. [17] and [20] showed that the phase of phosphors is related to the amount of H_3BO_3, and the amount of H_3BO_3 is not identical in Refs. [14] and [19] when the authors synthesized $Sr_4Al_{14}O_{25}$. These investigations may be more reasonable if the amount of H_3BO_3 is discussed. Consequently, it is necessary to study the required amount of H_3BO_3 when synthesizing pure phase $Sr_4Al_{14}O_{25}$. One role of the H_3BO_3 is as flux,[13–15,18,19] and the amount of H_3BO_3 should have relations to the weight of raw materials, so it is reasonable to use weight ratio to investigate the influence of H_3BO_3 to phosphors.

In this paper, different weights of H_3BO_3 were doped in samples, from 0% to 10%. By a little H_3BO_3 doping, Eu and Dy co-doped $Sr_4Al_{14}O_{25}$ pure phase was obtained and the effect of H_3BO_3 on the phase stability was studied. The photoluminescence and long afterglow characteristics of samples were carried out and the influence of the amount of H_3BO_3 on the luminescence properties of phosphors was discussed. All the samples show different persistence properties due to the different traps generated by the auxiliary activators. In order to study the relationships of the decay characteristics and

*Project supported by the National Natural Science Foundation of China (Grant Nos. 21271048, 11147152, and 61106124) and the Natural Science Fund of Zhanjiang Normal University of China (Grant No. QL1020).

†Corresponding author. E-mail: carlxw@163.com

© 2013 Chinese Physical Society and IOP Publishing Ltd

traps in the host matrix, we determine the trap depth and trap concentration by thermoluminescence measurement.

2. Experiments

2.1. Synthesis

All the phosphor samples were prepared by using the solid-state reaction method. Firstly, according to $Sr_{3.96}Al_{14}O_{25}$:$Eu^{2+}_{0.01}$,$Dy^{3+}_{0.02}$, stoichiometric composition of $SrCO_3$, Al_2O_3, Eu_2O_3, Dy_2O_3 were mixed and milled thoroughly in an agate mortar for 2 h. Then, the mixed powders were divided into five aliquots and different weights of H_3BO_3 (0%, 2%, 3%, 6%, and 10%) were added to each aliquot. All of these materials were of analytical purity. After mixing well, the powders were sintered at 1350 °C for 4 h with a weak reductive atmosphere of flowing 5%H_2+95%N_2. Finally, the phosphor samples were obtained, respectively. We named the samples according to the weight ratio of H_3BO_3: 0%(SAM1), 2%(SAM2), 3%(SAM3), 6%(SAM4), 10%(SAM5).

2.2. Measurement

The phase identification of the samples was carried out by powder XRD using a diffractometer with Cu Kα irradiation ($\lambda = 1.5406$ Å) at 36 kV tube voltage and 20 mA tube current at room temperature. The SEM analysis was conducted on a Philips XL-30 scanning electron microscope. The photoluminescence emission spectra were taken on a Hitachi F-7000 fluorescence spectrophotometer. Each sample was loaded into a circular holder and excited with 360 nm radiation from a pulsed xenon lamp. The emission spectra were scanned in the range of wavelengths from 400 nm to 600 nm. The decay curves were recorded by a GFZF-2A single-photon counter system. Prior to the decay curve measurements, the phosphors were excited by UV light for 5 min. The thermoluminescence curves were measured using a FJ427A1 thermoluminescent dosimeter. All the samples were excited by UV light for 5 min.

3. Results and discussion

3.1. XRD phase analysis

In order to determine the crystalline phase structure of samples, the XRD patterns were carried out. Figure 1 shows the XRD patterns of all the phosphors, respectively. In Fig. 1, the XRD patterns of the compounds are compared with the JCPDS standard values of suspected phases using different symbols. Figure 1(a) shows a mixture phases of monoclinic $SrAl_2O_4$ (JCPDS Card No. 34-0379) and hexagonal $SrAl_{12}O_{19}$(JCPDS Card No. 80-1195) in SAM1. However, with increasing H_3BO_3 content, XRD patterns start changing. The XRD pattern of SAM2 (Fig. 1(b)) shows some additional peaks, indicating the presence of another phase except $SrAl_2O_4$ and $SrAl_{12}O_{19}$. After comparison with JCPDS standard files, the extra peaks are identified as the reflections of orthorhombic $Sr_4Al_{14}O_{25}$ phase with the space group, *Pmma*. Some researchers[11] consider that the $Sr_4Al_{14}O_{25}$ phase is formed by the reaction of $SrAl_2O_4$ with the additional B_2O_3 which comes from H_3BO_3, and this phenomenon appeared again in SAM1 and SAM2. However, $Sr_4Al_{14}O_{25}$ pure single-phase is synthesized when the H_3BO_3 is 3 wt.% in SAM3 (Fig. 1(c)), all the peaks in Fig. 1(c) can be indexed based on the $Sr_4Al_{14}O_{25}$(JCPDS Card No. 74-1810) and hardly found any amorphous (glassy) phase. With the increase of H_3BO_3, $SrAl_{12}O_{19}$ is generated again on going to high H_3BO_3 contents in SAM4 (Fig. 1(d)) which is composited with 6 wt.% H_3BO_3. In Fig. 1(d), it can be seen that $Sr_4Al_{14}O_{25}$ appears as the major phase and $SrAl_{12}O_{19}$ as a minor phase. With increasing of H_3BO_3, the diffraction peaks of $SrAl_{12}O_{19}$ phase become higher in SAM5 (Fig. 1(e)) than that of SAM4 (Fig. 1(d)), which means the content of $SrAl_{12}O_{19}$ is rising in SAM5. From these observations, we believe that $Sr_4Al_{14}O_{25}$ pure phase cannot be synthesized without H_3BO_3, and the least amount of H_3BO_3 required to obtain $Sr_4Al_{14}O_{25}$ pure phase is 3 wt.%. When the content of H_3BO_3 is above 6%, other phases like $SrAl_{12}O_{19}$will exist. It is clear that H_3BO_3 plays an important role in synthesizing pure phase $Sr_4Al_{14}O_{25}$. H_3BO_3 is not only acting as flux, but also participates in the chemical reactions and affects the phases of the reaction product.

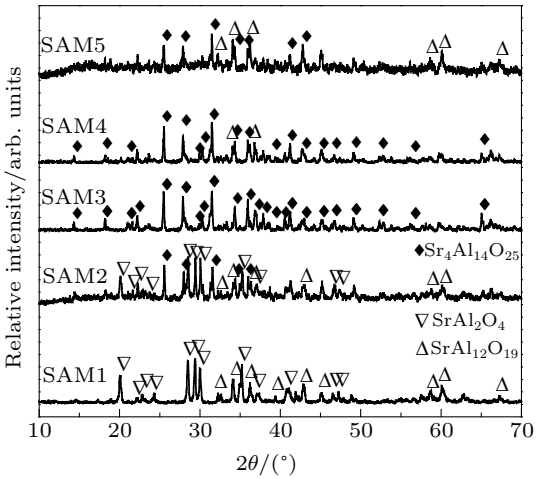


Fig. 1. The XRD patterns of the phosphors.

3.2. SEM analysis

An SEM study is carried out to investigate the surface morphology and the grain sizes of samples. The SEM micrographs of samples with different H_3BO_3 content (SAM1, SAM3 and SAM4) are shown in Fig. 2. It can be clearly seen from the Fig. 2(a) that SAM1 has irregular morphology with angularity and corners. There is a wide distribution of particles ranging from 2 μm to 6 μm observed in SAM1 (Fig. 2(a)). In contrast, the micrographs of SAM3 (Fig. 2(b)) exhibit particles with irregular lumps and smooth interfaces, and the grain size is bigger than that of SAM1, ranging from 5 μm to 20 μm.

This difference indicates that H_3BO_3 was added as flux; it provides a low melting medium for the solid/liquid reaction to proceed. With the increase of H_3BO_3, the presence of a glassy phase is clearer in SAM4 (Fig. 2(c)), the irregular particles of size ranging from 10 μm to 30 μm are embedded in a molten matrix and the surfaces of particles are very smooth.

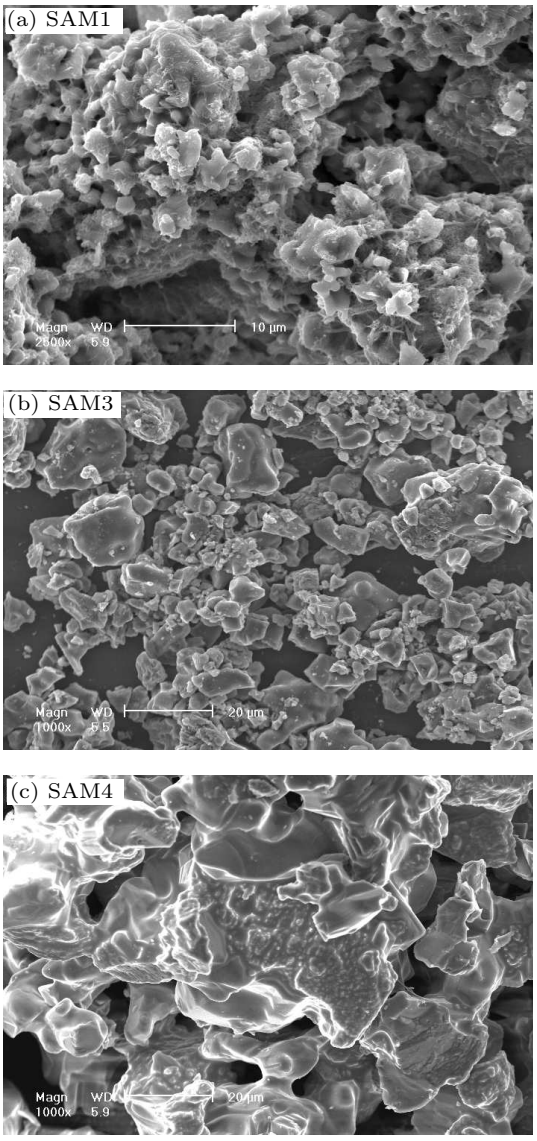


Fig. 2. Comparison of the SEM microstructure for (a) 0 wt.% H_3BO_3, (b) 3 wt.% H_3BO_3, and (c) 6 wt.% H_3BO_3.

When the phosphor is synthesized with H_3BO_3 at low content, it acts as flux, H_3BO_3 provides a melting medium for the solid-state reaction and quickens the rate of reaction, liquid interfaces are produced among crystal grains, and then the crystal grains reunite and result in the bigger particle size. When the phosphor is synthesized with H_3BO_3 at high content, the average grain sizes of samples continue to increase and the glassy phase is generated.

3.3. Spectral analysis

Figure 3 is the emission spectra of SAM3, SAM4, and SAM5 ($\lambda_{ex} = 360$ nm). The major phase of the three samples is $Sr_4Al_{14}O_{25}$. All the emission spectra show similar broadband emission peaks at about 490 nm from Eu^{2+}, which is due to the transitions of Eu^{2+} that originate from $4f^65d^1$ excitation state to $4f^7$ ground states.[15] It is obvious that with varying content of H_3BO_3, the position of the emission peak does not change, which suggests the crystal field is not changed much by the different composition of H_3BO_3. Chang[20] reported that the emission peak at about 486 nm shifts to the short wavelength side with the increase in B_2O_3content. This phenomenon did not happen in our results, presumably due to the variation of H_3BO_3 being very tiny in SAM3, SAM4, and SAM5. The emission spectra data is shown in Table 1.

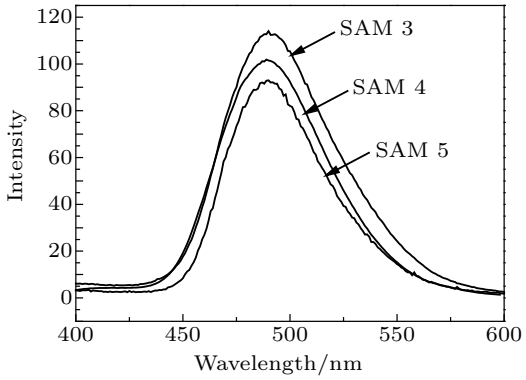


Fig. 3. Emission spectra of samples in $Sr_4Al_{14}O_{25}$ phase.

As can be seen from Table 1, the emission intensity of SAM3 is the highest one, SAM4 is in the middle, and the lowest is SAM5. However, the distinction of emission intensity is not obvious, which is the same as Ref. [20]. Compared with the results of Ref. [20], we hardly found any peak at 407 nm in Fig. 3; the explanation for this difference is that the 407-nm peak appears when the content of Eu^{2+}ions is 0.4%(mol), with increasing concentration of doped Eu^{2+}ions, the emission intensity of Eu^{2+} at 407 nm slowly decreases and completely vanishes as the concentration increases up to 1.2%(mol).[15] In this work, the concentration of Eu^{2+}ions is 1.0%(mol), just about 1.2%(mol), so the fact that we hardly found peaks at 407 nm is reasonable. In strontium aluminates, Eu^{2+} is the luminescence center after it replaces Sr^{2+},[21] and the ion concentration of the luminescence center has a great effect on the emission intensity. The emission intensity per one activator ion is given as follows:[22–24]

$$I/X = K[1 + \eta X^{Q/3}]^{-1}, \tag{1}$$

where x is the activator concentration, $Q = 6$, 8, or 10 means dipole–dipole, dipole–quadrupole, or quadrupole–quadrupole interaction, respectively, and K and η are contents for the same excitation conditions for a given host crystal. When x is very small, equation (1) can be reduced into

$$I/X = K, \tag{2}$$

so the ion concentration of the luminescence center is in direct proportion to the luminescence intensity. The relative content

of Eu^{2+} (assume the concentration in SAM3 is 1.0) shown in Table 1 is calculated using Eq. (2), and the distinction is not very large, that is corresponding to the distinction of emission intensity. Otherwise, it can be seen in Table 1 that the full width at half maximum (FWHM) of SAM5 is different from that of SAM3 and SAM4, indicating that the emission peak shape has changed with high H_3BO_3 content, which may be caused by the extra $SrAl_{12}O_{19}$ phase in SAM5.

Table 1. Emission spectra data of samples.

Sample	Position/nm	Area/a.u.	Relative content of Eu^{2+}	FWHM	Height
SAM3	490	7854.30	1.0	61	114
SAM4	489	6747.34	0.859	60	101
SAM5	490	5722.61	0.729	54	93

3.4. Decay characteristics

In order to confirm the luminescence center during afterglow phosphorescence, the typical time resolved phosphorescence spectrum of $Sr_4Al_{14}O_{25}$:Eu^{2+}, Dy^{3+} with 3% weight ratio doping of H_3BO_3 (SAM3), are shown in Fig. 4. The phosphorescence spectra were measured for every 5-min UV excitation at $\lambda = 360$ nm. The emission peak at about 490 nm in the afterglow phosphorescence remained the same with out any change, indicating that the 5d–4f transition of Eu^{2+}ions exists all the time during the decay of afterglow phosphorescence, thus the Eu^{2+}ion is the luminescence center during the decay process.

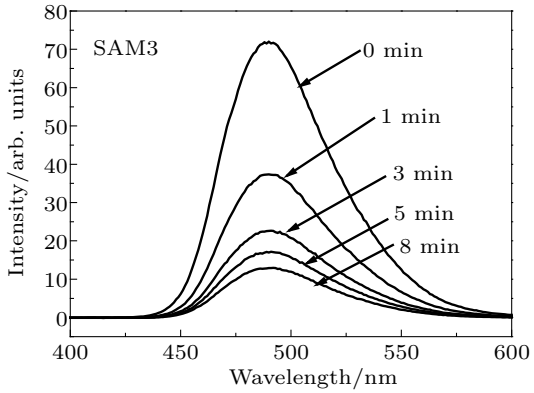


Fig. 4. Time-resolved phosphorescence spectra of $Sr_4Al_{14}O_{25}$: Eu, Dy phosphor with 3 wt.% H_3BO_3 which examined in 0, 1, 3, 5, 8 min after 360-nm UV light excitation for 5 min.

The decay curves of the phosphors are recorded after 5-min irradiation of UV light ($\lambda = 360$ nm). In order to study the effect of the varying content H_3BO_3 to phosphors, the decay curves of SAM1, SAM3, and SAM4 were shown in Fig. 5. All the decay curves contain a rapid-decaying process and a slow-decaying one, and the distinction of initial intensity is obvious. SAM3 shows the maximal intensity, SAM4 is in the middle, and the minimal one is SAM1. The afterglow characteristics were evaluated utilizing curve fitting.[13,16,25,26] The decay curves were fitted using double exponential equation

$$I = I_1 \exp\left(\frac{-t}{\tau_1}\right) + I_2 \exp\left(\frac{-t}{\tau_2}\right), \tag{3}$$

where I represents the phosphorescent intensity, I_1 and I_2 are two constants, t represents the time, τ_1 and τ_2 are decay constants which determine the decay rate for the rapid and slow exponentially decaying components. The fitting results of the parameters of τ_1 and τ_2 are listed in Table 2. It is obvious that the decay constants of SAM1 are much shorter than SAM3 and SAM4, indicating that the sample with the $Sr_4Al_{14}O_{25}$ phase shows superior decay characteristics. Compared with SAM3 and SAM4, SAM4 with 6 wt.% H_3BO_3 doping shows a longer decay time than SAM3 (3% doped H_3BO_3).

Table 2. The decay curve fitting results of the phosphor samples.

Sample	τ_1/s	τ_2/s
SAM1	4.56196	29.21862
SAM3	5.94878	42.39129
SAM4	8.09254	51.9223

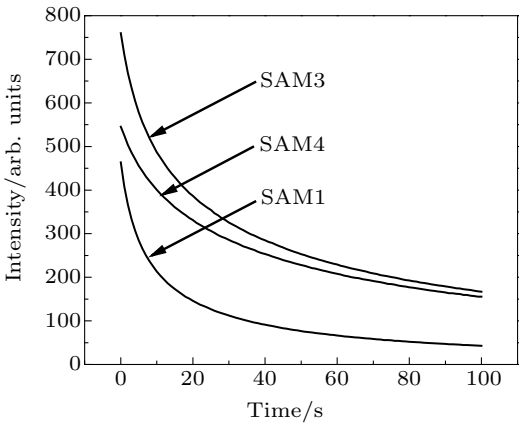


Fig. 5. Decay curves of the phosphors. (a) 0 wt.% H_3BO_3, (b) 3 wt.% H_3BO_3, and (c) 6 wt.% H_3BO_3.

3.5. Thermoluminescence

In general, the decay characteristics of phosphors are determined by the trap generated by the doped rare-earth RE^{3+}ions (RE = Dy, Nd, La, etc.),[27] and the trap is between the conduction band and valance band. The trap depth and trap concentrations have a great effect on the long afterglow properties. If the trap energy level is deeper and the number of the traps is larger, the afterglow time will become longer. However, the trap energy level should not be too deep because the energy may be too high to obtain by thermal agitation at room temperature and the afterglow cannot occur. On the other hand, if the depth of the trap levels is too shallow, the phosphor would show rapid decay and the phosphorescence would not last very long. It is necessary to examine whether various traps exist in our specimens. The thermoluminescence (TL) glow curves of these samples with different content of H_3BO_3 were given in Fig. 6. All the samples were irradiated by UV light, and the heating rate was controlled at 1 °C/s. From Fig. 6, we

can see that the curve of SAM1 is very different from SAM3 and SAM4 due to the different host phases, the former one shows a peak at 374 K, while SAM3 and SAM4 show peaks at about 396 K. Generally, the peak-shape method and the usual general order kinetics are used to describe TL curves. We can calculate the depth of traps and trap intensities according to the following equations:[28–32]

$$I(T) = sn_0 \exp\left(-\frac{E_t}{k_B T}\right) \times \left[\frac{(l-1)s}{\beta}\int_{T_0}^{T} \exp\left(-\frac{E_t}{k_B T}\right) dT + 1\right]^{-l(l-1)}, \quad (4)$$

where $I(T)$ is the TL intensity, n_0 is the concentration of trapped charges at $T = 0$, k_B is Boltzmann's constant, β is the heating rate (1 °C/s in this paper), E_t is the activation energy (or depth of the trap), s is the frequency factor, and l is the order of kinetics. Parameters E_t and n_0 are the most important parameters that describe the physical properties of the traps generated by the auxiliary activators. The frequency factor is obtained by taking the derivative of Eq. (6) with respect to T and setting it to zero at the peak temperature. The activation energy E_t (trap depth) and n_0 are calculated in terms of the glow-peak parameters by the following equation:[2,29,32]

$$E_t = [2.52 + 10.2(\mu_g - 0.42)]\left(\frac{k_B T_m^2}{\omega}\right) - 2k_B T_m, \quad (5)$$

$$n_0 = \frac{\omega I_m}{\beta}(2.52 + 10.2(\mu_g - 0.42)), \quad (6)$$

where ω is known as the shape parameter and defined as $\omega = \delta + \tau$, with δ being the high-temperature half width and τ being the low-temperature half width. The asymmetry parameter $\mu_g = \delta/\omega$. Calculated trap densities and the trap depth are shown in Table 3. From Table 3, the trap depth in SAM1 is 0.5 eV. The trap depth of SAM3 is slightly deeper than SAM4, indicating that with the increasing concentration of H_3BO_3 in $Sr_4Al_{14}O_{25}$, the trap depth becomes a little deeper, so the decay parameter of SAM4 is larger than that of SAM3.

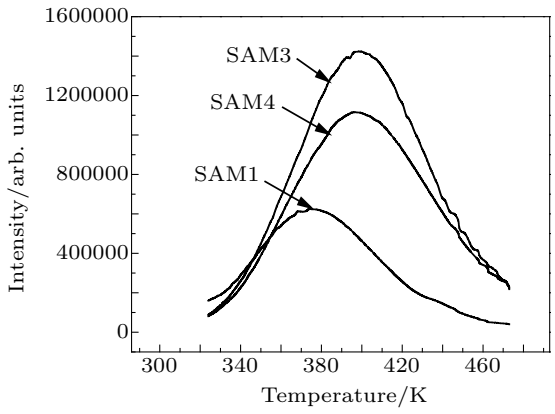


Fig. 6. The TL curves of the phosphors. (a) 0 wt.% H_3BO_3, (b) 3 wt.% H_3BO_3, and (c) 6 wt.% H_3BO_3.

In strontium aluminates, the doped Dy^{3+}(0.0912 nm) usually replaces Sr^{2+} (0.118 nm) due to the similar ion radius. In order to keep charge balance, two Dy^{3+}ions would replace three Sr^{2+} ions in the $Sr_4Al_{14}O_{25}$ matrix, so the vacancy is generated. During the solid-state reaction, H_3BO_3 decomposes to B_2O_3 in 165 °C, and the other components are in a liquid/solid state, so it is easy for ions to replace each other. Hence, if the H_3BO_3 content is higher, the replacement of Dy^{3+} and Sr^{2+} is easier, and this is beneficial to generate more lattice defects. Thus the trap become deeper. However, n_0 is another factor that can affect the afterglow characteristics, and can lead to high luminescence intensity when decay begins. In our samples, the n_0 value of SAM3 is the maximum (see Table 3), SAM4 in the middle, and the SAM1 is the minimum. These results are in good agreement with the result shown in decay curves. It indicates that with increasing content of H_3BO_3, the initial afterglow intensity first increases and then decreases. In this work, the phosphor synthesized with 3 wt.% H_3BO_3 shows the highest initial luminescence intensity.

Table 3. The parameters of the TL and the afterglow initial intensity for $Sr_4Al_{14}O_{25}$:Eu^{2+}, Dy^{3+} with different contents of H_3BO_3.

Sample	T_m/K	E_t/eV	$n_0/t = 0$	Initial intensity of afterglow
SAM1	374	0.500	1.2×10^7	463.4
SAM3	396	0.523	3.1×10^7	759.7
SAM4	397	0.529	2.4×10^7	545.2

4. Conclusions

The long afterglow phosphors $Sr_{3.96}Al_{14}O_{25}$:Eu^{2+}, Dy^{3+} with different contents of H_3BO_3 were synthesized successfully by using the solid-state reaction method. The $Sr_4Al_{14}O_{25}$ pure phase cannot synthesized without H_3BO_3. The $Sr_4Al_{14}O_{25}$ pure phase appears when the concentration of $H_3BO_3$is 3 wt.%, and whether the concentration of H_3BO_3 is lower or higher than 3 wt.%, the $SrAl_{12}O_{19}$ phase was generated. The grain size becomes bigger during the increase of H_3BO_3, and the surfaces of particles become smoother, because H_3BO_3 provides a melting medium for the solid-state reaction. The phosphor with 3 wt.% H_3BO_3 shows the highest emission intensity. However, the concentration of H_3BO_3 has a tiny influence on emission intensity and emission wavelength, suggesting that the crystal field is not changed much by the different composition of H_3BO_3. Phosphors with different concentrations of H_3BO_3 have different trap energy levels and different trap concentrations; with the increase of H_3BO_3, the traps become deeper, that is because a small amount H_3BO_3 is beneficial for ion replacement, which generates defects in the hosts. The sample with 3 wt.% H_3BO_3 shows excellent initial emission intensity due to the higher trap concentration, indicating that a small amount H_3BO_3 is helpful for the traps to capture the holes or electrons, and 3 wt.% is the best amount. This work studied the influence of H_3BO_3 on the phase stability and luminescence properties of $Sr_4Al_{14}O_{25}$:Eu^{2+}, Dy^{3+}.

The results indicate that $Sr_{3.96}Al_{14}O_{25}:Eu^{2+}$, Dy^{3+} with different concentration of H_3BO_3 can be used in various applications which need different luminescence intensities or afterglow times.

References

[1] Huang P, Cui C E and Wang S 2009 *Chin. Phys. B* **18** 4524

[2] Xie W, Wang Y H, Hu Y H, Wu H Y, Deng L Y and Liao F 2010 *Acta Phys. Sin.* **59** 1148 (in Chinese)

[3] Jiang Z Q, Wang Y H and Gong Y 2010 *Chin. Phys. B* **19** 027801

[4] Zhang J C, Qin Q S, Yu M H, Zhou H L and Zhou M J 2011 *Chin. Phys. B* **20** 094211

[5] Qiu J R, Miura K, Inouye H, Kondo Y, Mitsuyu T and Hirao K 1998 *Appl. Phys. Lett.* **73** 1763

[6] Peng T Y, Yang H P, Pu XL, Hu B, Jiang Z C and Yan C H 2004 *Mater. Lett.* **58** 352

[7] Xu X B, Zhou C L, He X H, Peng Z F and Yang S P 2004 *Mater. Lett.* **58** 1087

[8] Qiu Z F, Zhou Y Y, Lu M K, Zhang A Y and Ma Q 2007 *Acta Mater.* **55** 2615

[9] Metcalfe G D, Readinger E D, Shen H E, Woodward N T, Dierolf V and Wraback M 2009 *J. Appl. Phys.* **105** 053101

[10] Matsuzawa T, Aoki Y, Takeuchi N and Murayama Y 1996 *J. Electrochem. Soc.* **143** 2670

[11] Katsumata T, Nabae T, Sasajima K and Matsuzawa T 1998 *J. Cryst. Growth* **183** 361

[12] Nag A and Kutty T R N 2003 *J. Alloys Compd.* **354** 221

[13] Yuan Z X, Chang C K, Mao D L and Ying W J 2004 *J. Alloys Compd.* **377** 268

[14] Suriyamurthy N and Panigrahi B S 2008 *J. Lumin.* **128** 1809

[15] Lin Y H, Tang Z, Zhang Z and Nan C W 2002 *Appl. Phys. Lett.* **81** 996

[16] Chen R, Wang Y H, Hu Y H, Hu Z F and Liu C 2008 *J. Lumin.* **128** 1180

[17] Qiu G M, Chen Y J, Cui J Q, Geng X J, Wang H and Song B 2007 *J. Rare Earth* **25** 86

[18] Wu Z, Gong M L, Shi J and Su Q 2008 *J. Alloys Compd.* **458** 134

[19] Sharma S K, Pitale S S, Malik M M, Dubey R N and Qureshi M S 2009 *J. Lumin.* **129** 140

[20] Chang C K, Jiang L, Mao D L and Feng C L 2004 *Ceram. Int.* **30** 285

[21] Wang D, Yin Q, Li Y and Wang M 2002 *J. Lumin.* **97** 1

[22] Poort S H M, Blokpoel W P and Blasse G 1995 *Chem. Mater.* **7** 1547

[23] Van Uitert L G 1967 *J. Electrochem. Soc.* **114** 1048

[24] Ozawa L and Jaffe P M 1971 *J. Electrochem. Soc.* **118** 1678

[25] Sakai R, Katsumata T, Komuro S and Morikawa T 1999 *J. Lumin.* **85** 149

[26] Kubo H, Aizawa H, Katsumata T, Komuro S and Morikawa T 2005 *J. Cryst. Growth* **275** 1767

[27] Dorenbos P 2005 *J. Electrochem. Soc.* **152** H107

[28] Chen R 1969 *J. Electrochem. Soc.* **116** 1254

[29] Jahan M S, Cooke D W, Hults W L, Smith J L, Bennett B L and Maez M A 1990 *J. Lumin.* **47** 85

[30] Cooke D W, Bennett B L, Farnum E H, Hults W L, Muenchausen R E and Smith J L 1997 *Appl. Phys. Lett.* **70** 3594

[31] Forsythe E W, Morton D C, Tang C W and Gao Y 1998 *Appl. Phys. Lett.* **73** 1457

[32] Xie W, Wang Y H, Hu Y H, Zhang J, Zou C W, Li D and Shao L X 2011 *Acta Phys. Sin.* **60** 067801 (in Chinese)